Catalysis Today 177 (2011) 64–71

Contents lists available at ScienceDirect

Catalysis Today

journal homepage: www.elsevier.com/locate/cattod

Experimental and theory studies of the oxidation reaction of neutral gold carbonyl clusters in the gas phase

Yan Xie, Feng Dong, Elliot R. Bernstein*

Colorado State University, Department of Chemistry, Fort Collins, CO 80523-1872, USA

ARTICLE INFO

Article history:
Received 15 November 2010
Received in revised form 18 January 2011
Accepted 19 January 2011
Available online 8 March 2011

Keywords:
Gold clusters
Heterogeneous catalysis
Neutral clusters
Carbon monoxide oxidation
Relativistic effects
Theoretical calculations

ABSTRACT

Neutral gold carbonyl clusters, $Au_m(CO)_n$ ($m = 3–9$, $n = 2–7$, $m \geq n$), are generated by laser ablation of Au into a mixture of CO/He, cooled in a supersonic expansion, and reacted with O_2 and N_2O in a fast flow reactor. The neutral reactants and products are detected in a time of flight mass spectrometer through single photon ionization by a 193 nm laser. Signal intensities of $Au_3(CO)_{2,3}$, $Au_5(CO)_4$, and $Au_7(CO)_{4,5}$ decrease significantly following reaction of these clusters with O_2 in the fast flow reactor; only $Au_3(CO)_2$ and $Au_3(CO)_3$ signals decrease moderately following reaction with N_2O. The reaction cross section for $Au_m(CO)_n$ with N_2O is significantly smaller than that with O_2. Density functional theory calculations with and without explicit consideration of relativistic effects are performed to investigate the reaction mechanisms for the oxidation of $Au_3(CO)_2$ and $Au_3(CO)_3$ clusters with O_2 and N_2O. Both calculational algorithms predict a considerable barrier for the reactions of $Au_3(CO)_{2,3}$ with N_2O. Non relativistic density functional theory calculations predict a positive overall barrier for the reactions of $Au_3(CO)_{2,3}$ with O_2, in disagreement with experimental observations. Relativistic density functional theory calculations for the reactions $Au_3(CO)_{2,3}$ with O_2 predict that they are thermodynamically allowed, although the barrier heights are not in the appropriate order to support the apparent relative reactivities of $Au_3(CO)_2$ and $Au_3(CO)_3$ with O_2.

1. Introduction

Transition metals and metal oxides are widely employed as industrial heterogeneous catalysts, either alone or in mixtures. Gold based catalysts have been extensively used and studied for their unique activity for CO low temperature oxidation [1], NO reduction [2], and propene oxidation [3] on condensed phase surfaces and bulk phase solids [4–14]. Gas phase nano clusters can be good model systems for condensed phase bulk catalysts [15–18] because these species are readily accessible through theoretical calculations. Nano clusters can enable the identification of specific sites of reactivity for the bulk condensed phase and surface systems. Time of flight mass spectrometry (TOFMS) and infrared (IR) spectroscopy can also be employed for studies of reactions, structures, and electronic states of cationic [19–25] and anionic [15–18,26–34] gold clusters; theoretical calculations again are a specific aid to understanding and predicting the behavior of active and inactive nano cluster species [35–48]. Neutral gold clusters are less studied than ionic ones experimentally [49,50], particularly because neutrals must be ionized to detect, and ionization cross sections and fragmentation become critical issues for neutral cluster detection and identification. Additionally, neutral clusters are technically difficult to isolate, whereas ions can be readily selected and stored. The study of neutral gold clusters therefore heavily relies on quantum chemistry theory [37,41,51–59].

Carbon monoxide and oxygen adsorption and co-adsorption on neutral, anionic and cationic gold clusters have been explored experimentally [15–18,22–31,34,36,49,60,61] and theoretically [34–41,51–55,60–62] to generate a mechanism for the catalytic oxidation of CO to CO_2. CO and O_2 co-adsorption on an Au_n cluster is the key intermediate for CO oxidation. Au_n^- cluster anions with n even are found to be more reactive with O_2 in the gas phase than odd n cluster anions in a flow tube reactor, TOFMS study [26,63]. Photoelectron spectroscopy studies of Au_n^- cluster anions conclude that O_2 is chemisorbed on even n gold cluster anions, and physisorbed on odd n gold cluster anions [18]. CO adsorption on gold clusters under low and high CO exposure conditions is also reported [27]: a strong size dependent activity and saturation are found and these data could be employed to estimate Au_n cluster structure. Further experiments for CO and O_2 co-adsorption on Au_n^- cluster anions demonstrate that pre-adsorption of either CO or O_2 on Au_n^- species can increase the ability of the clusters to bind subsequent molecules. Interestingly, Au_6^- is the most active cluster anion for CO_2 generation [15]. Clusters $Au_2(CO)(O_2)^-$, $Au_3(CO)(O_2)^-$, and $Au_3(CO)(O_2)_2^-$ are observed for the co-adsorption of CO and O_2 on small cluster anions Au_2^-

* Corresponding author. Tel.: +1 970 491 16347; fax: +1 970 491 1801.
E-mail address: erb@lamar.colostate.edu (E.R. Bernstein).

0920-5861/$ – see front matter © 2011 Elsevier B.V. All rights reserved.
doi:10.1016/j.cattod.2011.01.047

and Au_3^- [16,30,60]. Saturated adsorption studies of CO on $Au_n^{\pm}$ cluster ions along with IR spectroscopy, have been used to explore the geometry of small gold cluster ions [23,32]. Chemisorption and physisorption of CO on anionic gold clusters have recently been explored by photoelectron spectroscopy and theoretical calculations by Wang et al. [64–67]. Chemisorption of CO on Au_n^- clusters occurs at low coordination apex sites: physisorption on these clusters has no apparent upper limit in principle. Kinetics experiments are performed for gold cation [22,24] and anion [31] clusters to estimate the binding energies of CO and O_2. In general, CO binding energies decrease with increasing cluster size from 1.1 eV to 0.65 eV for Au_n^+ clusters (n = 6–65) [24]. CO adsorption on neutral gold clusters, Au_n (n = 9–68), has been studied and a strong cluster size dependence is found for clusters with up to four CO molecules attached [49]. Comparisons between ionic and neutral Au_n cluster behavior show that both similarities and differences are found for the reactions of CO with neutral and ionic gold clusters: the number of valence electrons, rather than the number of gold atoms, plays a role in the neutral and ionic gold cluster chemistry.

Many theoretical studies have appeared for CO and O_2 adsorption on gold clusters. Relativistic effects must be considered for these systems since gold is a heavy metal with an electronic configuration $[Xe]4f^{14}5d^{16}6s^1$ [33,68–76]. Implicit inclusion of some relativistic effects on cluster energy, structure, and chemistry can be incorporated into density functional theory (DFT) calculations through the use of effective core potential basis sets for gold atoms, such as LANL2DZ [77]. Explicit inclusion of relativistic effects into a DFT algorithm can be further modeled with the addition of spin orbit and scalar terms to the Hamiltonian [78]. We refer to DFT calculations with only effective core potentials for Au calculations as NRDFT and to DFT calculations with both implicit and explicit inclusion of relativistic effects for Au atoms as RDFT calculations. NRDFT calculations are reported for CO on small $Au_n^{0,\pm}$ (n = 1–6): geometry optimization suggests that bare gold clusters and CO adsorbed clusters in this size range prefer planar structures, unrelated to the charge state of the cluster. CO binding at an "on top" site (in the plane) is the most favorable conformation, with binding energies in the order $Au_n^+ > Au_n^0 > Au_n^-$ [39]. A two dimensional (2D) to three dimensional (3D) transition for cationic gold clusters occurs between Au_8^+ and Au_9^+, while the 2D to 3D transition for neutral gold clusters occurs between Au_{10} and Au_{11}, based on NRDFT calculations [42]. The 2D to 3D transition at neutral Au_{14} has also been examined [56]. Comparisons of different DFT methods for study of Au_{2-5} are also reported recently, which include scalar and spin orbit coupling effects [58]. O_2 is predicted to be more weakly bonded to neutral gold clusters than to anionic gold clusters. Molecular adsorption is calculated to be more stable than dissociative adsorption on a neutral gold atom, whereas dissociative adsorption is more stable than molecular adsorption on an anionic gold atom [36]. Experimental and theoretical studies are further focused on AuO_2^- and only a linear $OAuO^-$ structure is observed and predicted [79].

To date, no experimental results are reported for the co-adsorption of CO and O_2 on neutral gold clusters, and only a few calculations for this system are reported for CO catalytic oxidation to CO_2 on neutral gold clusters [41]. In this report, small neutral gold and gold carbonyl clusters are generated by laser ablation of gold and reacted with O_2 and N_2O in a high pressure (10–50 torr) fast flow reactor following supersonic expansion. Reactants and products are ionized by 193 nm single photon ionization (SPI). Gold carbonyl cluster oxidation with O_2 is observed for small gold clusters, and theoretical DFT calculations for the reaction pathways, generally agree with experimental observations and explain the reactivity of $Au_m(CO)_n$ with O_2 and the non-reactivity of $Au_m(CO)_n$ with N_2O. A catalytic cycle is proposed to explain the condensed phase $Au/CO/O_2$ behavior based on the experimental and theoretical results generated in the gas phase study.

2. Procedures

2.1. Experimental

The apparatus used for the present experiments is a TOFMS coupled with SPI at 193 nm as described in our previous publications [80,81]. $Au_m(CO)_n$ clusters are generated in a laser ablation source. A gold foil (Sigma Aldrich, dia. 12 mm disk and 0.127 mm thickness) is used for laser ablation and a 5% CO/He gas mixture is used for the expansion gas at 80 psi backing pressure. The ablation laser source is a focused, second harmonic 532 nm Nd^{3+}:YAG laser with a 10 Hz repetition rate and ca. 7 mJ/pulse energy. Reactions of $Au_m(CO)_n$ clusters with O_2 and N_2O occur in a fast flow reactor, which is directly connected to the laser ablation head. The reactant gases are pulsed into the reactor by a general valve and the timing sequences are optimized for best product yield. After removal of ions from the molecular beam by an electric field, reacted and un-reacted neutral clusters are skimmed into a second vacuum chamber containing the TOFMS detection system. An unfocused 193 nm laser beam is employed for the ionization, and the laser fluence is set to ca. 150 $\mu J/cm^2$ to avoid severe multi photon fragmentation of reactants and products. Mass spectra are detected by a multi channel plate (MCP) detector and are recorded and stored by a digital storage oscilloscope.

2.2. Calculational

The structures and energies for the neutral gold carbonyl clusters and their reaction intermediates, transition states, and products are calculated by Gaussian 03 [77] and the Amsterdam Density Functional (ADF) [78] programs. Gaussian calculations are carried out with Becke's exchange and Perdew–Wang correlation functional coupled with a Los Alamos effective core potential plus a double zeta basis set for gold atoms and the standard 6-311+G(d) basis set for carbon and oxygen atoms. ADF calculations are performed employing the generalized gradient approximation of Perdew–Wang 1991 and triple zeta Slater basis sets plus p- and f-polarization functions (TZ2P) for gold, carbon, and oxygen atoms. Scalar relativistic effects are explicitly taken into account through the zero order regular approach (ZORA) within the ADF algorithm. These two programs are employed to generate non relativistic (NRDFT) calculational results (Gaussian 03) and relativistically corrected (RDFT) calculational results (ADF). The two different algorithms are employed to compare the effects of explicit relativistic corrections on the reaction potential energy surfaces (PESs), and cluster structures and energies. Note that both NRDFT and RDFT calculations use effective core potentials for Au basis functions, and thereby implicit relativistic parameters are employed in both NRDFT and RDFT calculations. Some calculations with explicit inclusions of spin orbit effects are performed to test the importance of this contribution to the reaction potential energy surface and cluster structure.

The calculations for the PESs of the reactions of gold carbonyls with O_2 and N_2O involve the geometry optimizations for all reactants, intermediates, and products. Vibrational frequencies are further checked to obtain the zero point correction (ZPE) and reaction enthalpies, and to confirm the global minima ground states and transition states, which have zero and one imaginary frequency, respectively. Moreover, intrinsic reaction coordinate (IRC) calculations are performed to determine that the candidate transition state connects two appropriate local minima along the reaction pathways.

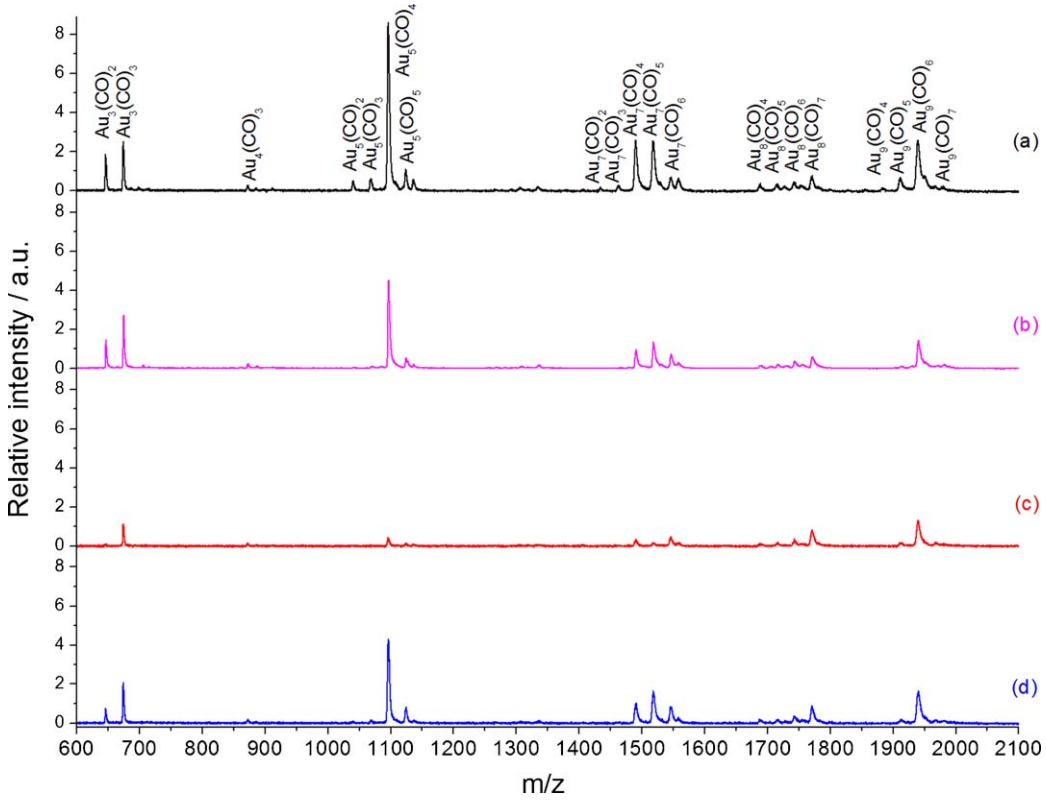

Fig. 1. Neutral $Au_m(CO)_n$ cluster distribution after reaction with (a) pure helium, (b) 5% N_2/He, (c) 5% O_2/He, and (d) 5% N_2O/He in a fast flow reactor, detected by 193 nm laser single photon ionization.

3. Results and discussion

3.1. Experimental

Ionization energies of small Au_{1-9} neutral clusters are all higher than the 6.4 eV (193 nm) ionization photon energy; therefore, these pure gold clusters are not observed by 193 nm SPI. The fact that they are not observed, moreover, supports the SPI mechanism conditions for the present experiments. The ionization energies of gold carbonyl clusters, however, are less than those of pure gold clusters and these clusters can be ionized by 6.4 eV photons. The cluster distributions with a 5% CO/He expansion gas and different gases (e.g., He, O_2/He, N_2/He, and N_2O/He) in the reactor are presented in Fig. 1. Traces a and b of Fig. 1 show the cluster distribution with He and 5% N_2/He in the reactor as a comparison for cluster signal reduction upon scattering vs. cluster signal reduction due to reaction, as in traces c and d for 5% O_2/He and 5% N_2O/He. In general, one sees immediately from these traces that N_2 scatters (un-reactively) $Au_m(CO)_n$ clusters to reduce their overall intensity, O_2 reacts with $Au_m(CO)_n$ clusters to reduce their intensity beyond expectations for scattering, and N_2O is not very reactive, if at all, with $Au_m(CO)_n$ clusters.

Multiple CO adsorption products, specifically, $Au_3(CO)_{2,3}$, $Au_4(CO)_3$, $Au_5(CO)_{2-5}$, $Au_7(CO)_{2-6}$, $Au_8(CO)_{4-7}$, and $Au_9(CO)_{4-7}$ are detected in the mass spectrum of Fig. 1a. No gold/CO clusters are found for Au, Au_2, and for $Au_{3-9}(CO)_{0,1}$, because their ionization energies are calculated (NRDFT) to be greater than 6.4 eV. For example, the ionization energies of $Au_3(CO)$ and $Au_5(CO)$ are estimated at 7.09 and 6.75 eV, respectively, while those for $Au_3(CO)_2$, $Au_3(CO)_3$, and $Au_5(CO)_4$ are estimated to be 6.35, 5.89, and 5.64 eV, respectively. As can be seen from trace a of Fig. 1, these calculated ionization energies agree with the experimental results.

Calculated structures for $Au_3(CO)$, $Au_5(CO)$, $Au_3(CO)_2$, $Au_3(CO)_3$ and $Au_5(CO)_4$ are estimated as planar in both the ground neutral and ion states, by both RDFT and NRDFT. The $Au_m(CO)_n$ clusters synthesized in the ablation/expansion process should be formed under saturated conditions and are listed in Table 1 for $Au_m(CO)_n$, with $m = 3–9$. These are also compared with ionic clusters found and characterized in previous studies. The neutral and ionic clusters differ only for Au_4 and Au_9: $Au_4(CO)_3^0$ vs. $Au_4(CO)_4^+$ and $Au_9(CO)_7^0$ vs. $Au_9(CO)_8^+$ probably because the signals of $Au_4(CO)_4$ and $Au_9(CO)_9$ are too weak to detect as shown in Fig. 1a. Fewer CO molecules can adsorb to anionic gold clusters than either neutral or cationic gold clusters. These differences between clusters of various charge states have been studied and determined through both theory and experiment [23,27,32].

The reactions of $Au_m(CO)_n$ ($m = 3–9$, $n = 2–7$, $m \geq n$) with 5% O_2/He and 5% N_2O/He are studied and the results are presented in

Table 1
Observed saturation compositions of $Au_m(CO)_n^{0,\pm}$ (m, n) clusters.[a]

m	Neutrals		Cations	Anions	
	n_{max}	other n	n_{max}[b]	n_{max}[c]	n_{max}[d]
3	3	2	3	–	≥1
4	3	–	4	–	4
5	5	2–4	5	4	4
6	–	–	6	4	6
7	6	2–5	6	4	4
8	7	4–6	7	5	4
9	7	4–6	8	6	6

[a] Only chemisorption of CO is considered; physisorption has no upper limit in principle, see Refs. [64–67] for more details.
[b] Ref. [23].
[c] Ref. [27].
[d] Ref. [32].

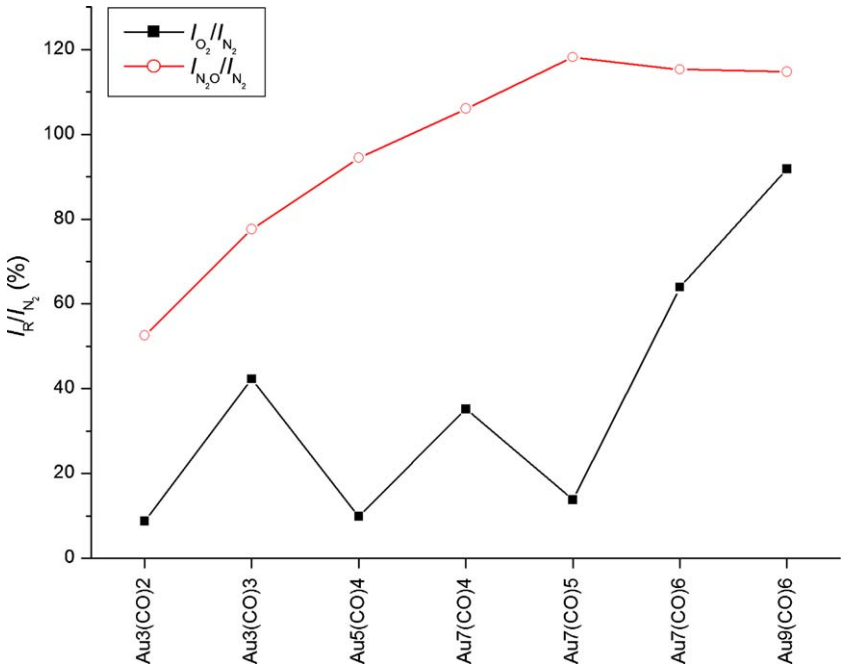

Fig. 2. Signal intensity ratios for selected $Au_m(CO)_n$ clusters after reactions with O_2 and N_2O as normalized by the N_2/He signal to account for cluster scattering. Due to signal weakness in some reactions, and differences in fast flow reactor pressures and timing, an error of ±10 to 15% for these values is reasonable. Note that scattering effects for N_2O samples could be more significant for the lighter, smaller clusters than for the heavier, larger ones.

Fig. 1c and d. In general, all cluster signals decrease significantly following reaction with O_2; they are still intense following reaction of the clusters with N_2O. These signal changes are best compared to those of Fig. 1b for $Au_m(CO)_n$ scattered by N_2/He in the reaction flow cell. Fig. 2 presents the relative intensities of the signals as I_{O_2}/I_{N_2} and I_{N_2O}/I_{N_2}: as can be seen in this graph, $Au_m(CO)_n$ neutral clusters are much more reactive with O_2 than with N_2O. The decrease of $Au_m(CO)_n$ signals probably be ascribed to the following reactions: $Au_m(CO)_n + O_2 \rightarrow AuO(CO)_{n-1} + CO_2 \rightarrow Au_m(CO)_{n-2} + 2CO_2$ and $Au_m(CO)_n + N_2O \rightarrow Au_m(CO)_{n-1} + CO_2 + N_2$.

As a comparison experiment, neutral Au_mO_n clusters are generated by laser ablation of gold into 5% O_2/He, expansion cooled, and are passed through the fast flow reactor with 5% CO/He; however, only $Au_m(CO)_n$ clusters are detected in this configuration. Au_mO_n clusters are not detected by either 6.4 eV or 10.5 eV (118 nm) SPI: the 10.5 eV photon should ionize at least some Au_mO_n neutral clusters with relatively low ionization energy, and thus one can conclude that they are not formed in the expansion source. A gas mixture of CO and O_2 in the reactor also reacts with Au_m clusters from the ablation/expansion source with similar results to the reactions depicted in Fig. 1. The conclusion from these studies is therefore that the reaction of CO oxidation by O_2 on neutral gold clusters involves CO adsorption followed by O_2 adsorption. This conclusion is different from that drawn from Au_n^- cluster anion studies, in which either CO or O_2 pre-adsorption can increase the association of CO and O_2 to generate CO_2 [15]. To understand further the mechanisms of CO oxidation on gold clusters by either O_2 or N_2O, the PESs for the oxidation reactions of small clusters $Au_3(CO)_2$ and $Au_3(CO)_3$ are investigated through both RDFT and NRDFT calculations.

3.2. Potential energy surface calculations

3.2.1. $Au_3(CO)_2 + O_2$

The catalytic reactions of $Au_3^{0,\pm}$ clusters have been studied theoretically, including: (1) H_2O_2 formation from H_2 and O_2 [57]; (2) partial oxidation of propylene to propylene oxide [59]; and (3) CO oxidation to CO_2 by O_2 [41]. Wang et al. calculated and suggested three reaction pathways for the $Au_3^{0,\pm} + 2CO + O_2$ reaction [41]; however, none of those channels involves O_2 attacking $Au_3(CO)_2$, which is the initial reactant for the data reported in Fig. 1a. Fig. 3 presents the reaction pathways for the reaction $Au_3(CO)_2 + O_2 \rightarrow Au_3(CO)_2O_2 \rightarrow Au_3O(CO) + CO_2 \rightarrow Au_3 + 2CO_2$. O_2 is first adsorbed to $Au_3(CO)_2$ by bonding to a carbon atom in a CO moiety (the association energy is estimated as −3.8 and −8.1 kcal/mol by NRDFT and RDFT, respectively. (All values mentioned below and separated by a forward slash are NRDFT/RDFT results.) The intermediate **I1** is not the global minima for the O_2 associated structure; the structure of O_2 adsorbed on the non-coordinated Au is the lowest energy structure for $Au_3(CO)_2O_2$ with association energy −13.4/−25.8 kcal/mol; however, the lowest energy structure does not lead to CO oxidation to CO_2. Bond lengths for the O–O and O–CO bond for reaction intermediate **I1** in Fig. 3 are calculated at 1.311/1.319 Å and 1.598/1.578 Å, respectively. For a reference, the O–O bond length is estimated at 1.221/1.223 Å for a free O_2. RDFT predicts a longer O–O bond length, a shorter O–CO bond length, and a tighter bonding between O_2 and $Au_3(CO)_2$ compared to NRDFT. Following a structural rearrangement, an O–O–C–Au four membered ring forms for the structure **I2**, through transition state **TS1**, with an energy of 4.9/−2.2 kcal/mol. Intermediate **I2** can surmount an overall barrier **TS2** (8.8/0.6 kcal/mol), to form reaction intermediate **I3**, in which a CO_2 moiety is formed and weakly bonded to the $Au_3O(CO)$ cluster. The first CO_2 molecule can be released (**I4**) and the second CO_2 molecule forms through the transition state **TS3** for an internal oxygen transfer (**I5**) with energy far below the initial reaction energy (−26.9/−29.4 kcal/mol). The pure metal cluster Au_3 and two CO_2 molecules are generated as final products.

Ionization energies for reaction intermediates **I1**, **I2**, **I3**, **I4** are calculated as 8.31/8.47, 8.02/7.97, 8.42/8.46 and 8.40/8.43 eV, respectively, which are all much higher than the SPI of 6.4 eV (at 1.5×10^{14} photons/pulse); therefore, no mass peaks associated with these species can be observed. These species are not detected by 118 nm (10.5 eV) radiation, for which only 6×10^{11} photons/pulse are available. They may also be too short lived to detect under the experimental conditions. Since the signal

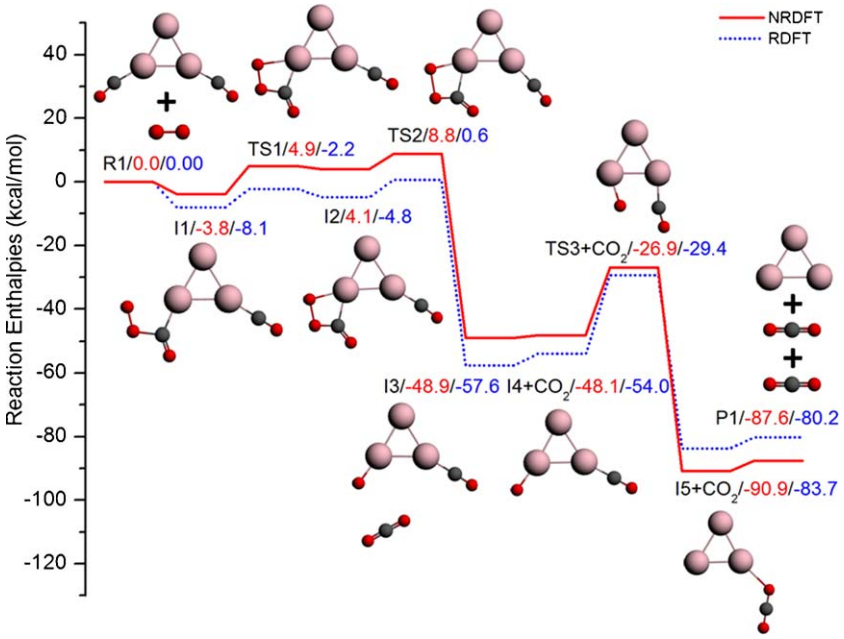

Fig. 3. Potential energy surface calculations for the reaction $Au_3(CO)_2 + O_2 \rightarrow Au_3 + 2CO_2$ employing NRDFT (red solid line) and RDFT (blue dot line). Energy level labels A/B/C in the figure denote the following: A represents reactants (R), products (P), intermediates (I) and transition states (TS); B represents energy difference relative to the initial reactant energy (R) calculated by NRDFT; and C represents energy difference relative to the initial reactant energy (R) calculated by RDFT. (For interpretation of the references to colour in this figure legend, the reader is referred to the web version of the article.)

for $Au_3(CO)_2$ decreases ca. 90% after reaction with O_2, this suggests that the reaction goes to completion. Final product CO_2 cannot be detected by 6.4 eV or 10.5 eV SPI, and product Au_3 has a high ionization energy and a weak signal for 10.5 eV ionization at ca. 1 μJ/pulse. The NRDFT calculation predicts this reaction will not surmount the **TS1** barrier; this result is inconsistent with the above data. RDFT calculations predict a ca. 0.6 kcal/mol barrier for the reaction; thus, the reaction is calculated to be thermodynamically allowed under "explicit incorporation of scalar relativistic effects" for the PES. An extended RDFT calculation can also been performed to include spin orbit coupling in the relativistic algorithm. Such inclusion increases the calculation time dramatically, but has only a small effect on the barrier heights (for example, **TS2** is at 0.1 kcal/mol with spin orbit plus the scalar relativistic corrections vs. 0.6 kcal/mol with only the scalar relativistic correction, relative to the reactants) and cluster structures for the $Au_3(CO)_2 + O_2$ reaction.

3.2.2. $Au_3(CO)_3 + O_2$

The potential energy path for the reaction $Au_3(CO)_3 + O_2 \rightarrow Au_3(CO) + 2CO_2$ is shown in Fig. 4. The structures and energy differences for the reaction of $Au_3(CO)_3$ with O_2 are similar to those for the reaction of $Au_3(CO)_2$ with O_2 given in Fig. 3, except that an extra CO is bonded to the un-coordinated Au atom of $Au_3(CO)_2$. The association energy of O_2 with $Au_3(CO)_3$

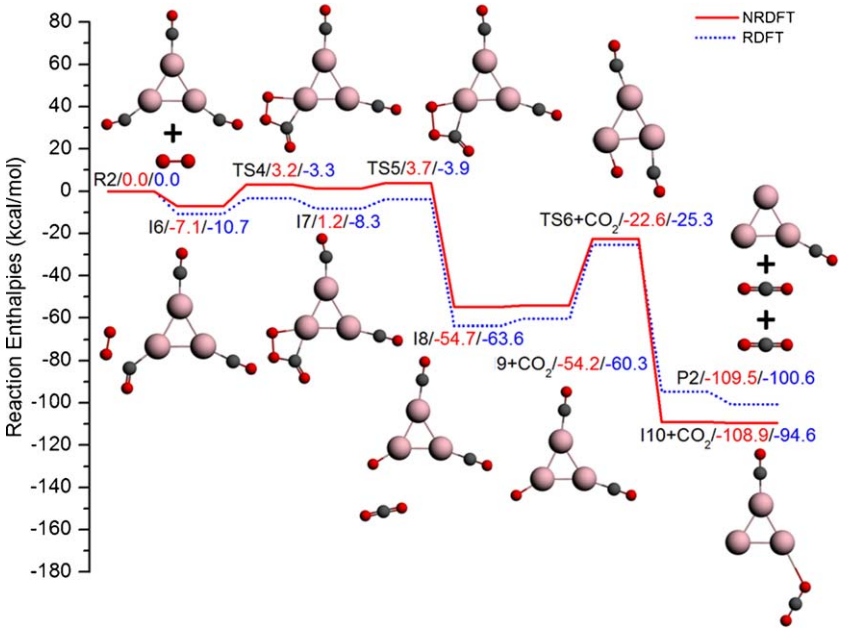

Fig. 4. Potential energy surface calculations for the reaction $Au_3(CO)_3 + O_2 \rightarrow Au_3(CO) + 2CO_2$ employing NRDFT (red solid line) and RDFT (blue dot line). See Fig. 3 caption for notation details. (For interpretation of the references to colour in this figure legend, the reader is referred to the web version of the article.)

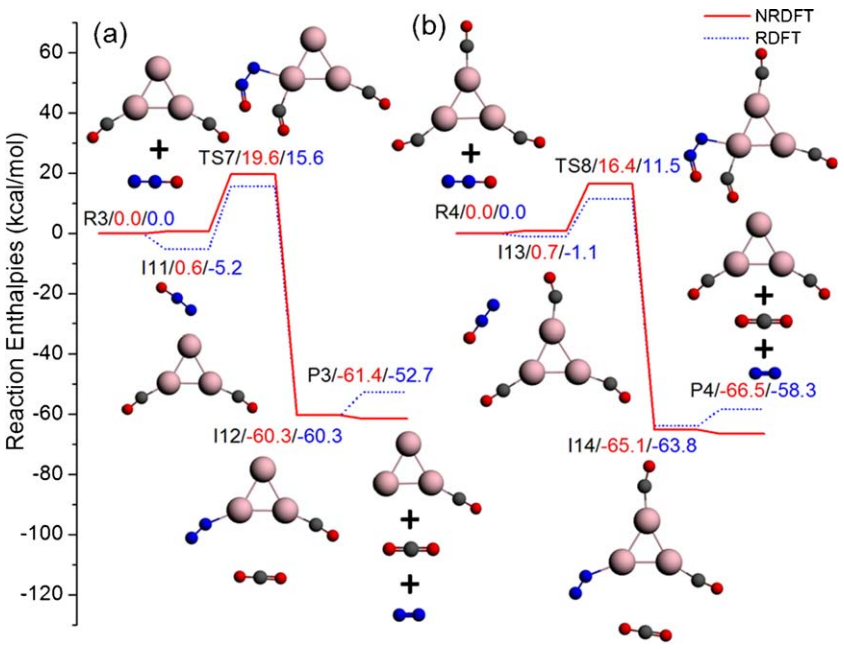

Fig. 5. Potential energy surface calculations for the reactions (a) $Au_3(CO)_2 + N_2O \rightarrow Au_3(CO) + CO_2 + N_2$ and (b) $Au_3(CO)_3 + N_2O \rightarrow Au_3(CO)_2 + CO_2 + N_2$ by employing NRDFT (red solid line) and RDFT (blue dot line). See Fig. 3 caption for notation details. (For interpretation of the references to colour in this figure legend, the reader is referred to the web version of the article.)

(reaction intermediate **I6**) is estimated to be −7.1/−10.7 kcal/mol, which is slightly larger than that for O_2 bound to $Au_3(CO)_2$. The bond lengths O–O and O–CO in the structure **I6** are calculated at 1.300/1.315 and 1.672/1.578 Å, respectively. The O–O bond length is similar to that in the structure **I1** (1.311/1.319 Å) whereas the O–CO bond length is longer than/equal to that in structure **I1** (1.598/1.578 Å). The NRDFT result for the O–CO bond length is considerably longer than the RDFT result: moreover, the NRDFT O–CO bond lengths for the two clusters ($Au_3(CO)_{2,3}O_2$, **I1**, **I6**) are also quite different. The ionization energies of **I6** and **I7** are predicted to be 7.80/8.05 and 7.59/7.60 eV, and thus these species are not observed for 193 nm SPI detection. Again since the intermediate species are not detected by 193 or 118 nm SPI, the reaction probably goes to completion, with final product $Au_3(CO) + 2CO_2$. The transition states **TS4** for the structure rearrangement and **TS5** for the first CO_2 release are slightly lower in energy than those (**TS1** and **TS2**) for the reaction of $Au_3(CO)_2$ with O_2: the first CO_2 molecule is more easily generated on $Au_3(CO)_3$ than on $Au_3(CO)_2$. Transition state **TS6** is slightly higher in energy than **TS3**, supporting the idea that the second CO_2 generated is more easily done on $Au_3(CO)_2$. The overall reaction barrier for the $Au_3(CO)_3 + O_2$ reaction is 3.7 kcal/mol by NRDFT and −3.9 kcal/mol by RDFT calculations. Again, explicit incorporation of relativistic effects for the reaction potential energy pathway is necessary to predict an overall thermodynamically allowed reaction.

3.2.3. $Au_3(CO)_{2,3} + N_2O$

The PES pathways for the reactions $Au_3(CO)_2 + N_2O \rightarrow Au_3(CO) + CO_2 + N_2$ and $Au_3(CO)_3 + N_2O \rightarrow Au_3(CO)_2 + CO_2 + N_2$ are calculated as above and displayed in Fig. 5a and b, respectively. Both NRDFT and RDFT estimate positive overall barriers for these two oxidation reactions: 19.6/15.6 kcal/mol for the reaction of $Au_3(CO)_2$ with N_2O; and 16.4/11.5 kcal/mol for the reaction of $Au_3(CO)_3$ with N_2O. Thus, both $Au_3(CO)_{2,3}$ oxidations by N_2O are thermodynamically unfavorable. The association energy N_2O with $Au_3(CO)_2$ is greater than that with $Au_3(CO)_3$, because N_2O bonds to the uncoordinated Au atom in the neutral cluster (**I11** and **I13**). The five membered ring transition states **TS7** and **TS8** are key steps in the formation of a CO_2 molecule. **TS7** is higher in energy than **TS8**, 19.6/15.6 vs. 16.4/11.5 kcal/mol, respectively. The energy difference for the overall barriers for the reactions of $Au_3(CO)_2$ and $Au_3(CO)_3$ with N_2O is the same as that for the reactions with O_2: **TS2** is higher in energy than **TS5**, as shown in Figs. 3 and 4.

3.3. Proposed catalytic cycles

Reaction of neutral gold clusters with CO also occurs at low temperatures (ca. 300–400 K): CO is pulsed into the fast flow reactor and reacts with neutral gold clusters. $Au_m(CO)_n$ clusters, including $Au_3(CO)_2$ and $Au_3(CO)_3$ are observed in the mass spectra, but are not as abundant as those generated in the reaction with CO seeded in the expansion gas (high temperature). Moreover, the signal intensities of the $Au_m(CO)_n$ clusters are weaker than those of $Au_m(CO)_{n-1}$ cluster. This observation indicates that CO adsorption reactions occur in the reactor at near room temperature.

Clusters $Au_3(CO)_2$ and $Au_3(CO)_3$ can be oxidized by O_2 to the products Au_3 and $Au_3(CO)$ as presented in Figs. 3 and 4. The Au_3 cluster can further react with two CO molecules to regenerate $Au_3(CO)_2$; $Au_3(CO)$ can react with another one or two CO molecules to generate $Au_3(CO)_2$ or $Au_3(CO)_3$, or $Au_3(CO)$ can be directly oxidized to Au_3 plus CO_2. Therefore, a catalytic cycle for CO oxidation to CO_2 on an Au_3 cluster surface by O_2 can be proposed. Fig. 6 presents a diagrammatic representation of the implied reactions. The catalytic cycle incorporates the following reactions:

(1) Adsorption

$$Au_3 + 2CO \rightarrow Au_3(CO)_2 \quad (1a)$$

$$Au_3 + 3CO \rightarrow Au_3(CO)_3 \quad (1b)$$

(2) Reaction

$$Au_3(CO)_2 + O_2 \rightarrow Au_3O(CO) + CO_2 \rightarrow Au_3 + 2CO_2 \quad (2a)$$

$$Au_3(CO)_3 + O_2 \rightarrow Au_3O(CO)_2 + CO_2 \rightarrow Au_3(CO) + 2CO_2 \quad (2b)$$

(3) Regeneration

$$Au_3(CO) + CO \rightarrow Au_3(CO)_2 \quad (3a)$$

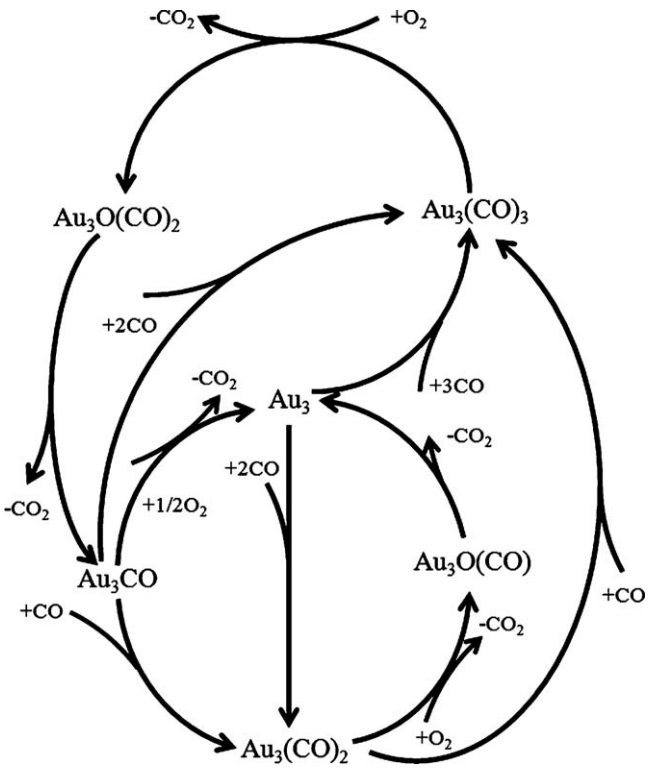

Fig. 6. Schematic representation of the catalytic cycle for CO oxidation to CO_2 by O_2 on the Au_3 cluster. Similar cycles can be expanded for odd number Au_m in general, as appropriate.

$$Au_3(CO) + 2CO \rightarrow Au_3(CO)_3 \quad (3b)$$

$$2Au_3(CO) + O_2 \rightarrow 2Au_3 + 2CO_2 \quad (3c)$$

Note that the catalytic cycle presented in Fig. 6 is not only for Au_3: for example, clusters $Au_5(CO)_4$ and $Au_7(CO)_5$ react with O_2, indicating that the Au_5 and Au_7 clusters are probably also potential catalysts for the CO oxidation reaction to CO_2. Thus, one can conjecture that most, if not all, odd Au_m neutral species can potentially catalyze the oxidation of CO to CO_2.

4. Conclusions

$Au_3(CO)_2$, $Au_5(CO)_4$ and $Au_7(CO)_5$ neutral clusters are especially reactive with O_2 and neutral clusters $Au_3(CO)_3$ and $Au_7(CO)_4$ are only moderately reactive with O_2. In general, with possible minor exceptions for $Au_3(CO)_2$ and $Au_3(CO)_3$, none of the $Au_m(CO)_n$ neutral clusters studied in these experiments prove to be reactive with N_2O. DFT calculational methods both with and without explicit relativistic corrections, RDFT and NRDFT, respectively, are employed to explicate this behavior. Both calculational approaches estimate overall positive barriers for the reactions $Au_3(CO)_{2,3} + N_2O \rightarrow Au_3(CO)_{1,2} + CO_2 + N_2$. The apparent small reactivity of $Au_3(CO)_{2,3}$ with N_2O (decrease in normalized scattering) can then be ascribed to clusters at higher temperatures than 300 K, and/or increased collisional non-reactive scattering between $Au_3(CO)_{2,3}$ and N_2O with respect to that between $Au_3(CO)_{2,3}$ and N_2.

Positive overall barriers are estimated by NRDFT calculations for the reactions $Au_3(CO)_2 + O_2 \rightarrow Au_3(CO) + CO_2 \rightarrow Au_3 + 2CO_2$ and $Au_3(CO)_3 + O_2 \rightarrow Au_3O(CO)_2 + CO_2 \rightarrow Au_3(CO) + 2CO_2$. These positive barriers are not consistent with the facile reactions observed for those clusters with O_2. On the other hand, the RDFT results predict that these $Au_m(CO)_n$ reactions with O_2 are thermodynamically accessible at 300 K with barrierless mechanisms. These results suggest that relativistic effects are an important component of the reactivity of $Au_m(CO)_n$ clusters toward O_2. Nonetheless, the RDFT algorithm may not yet be perfected with regard to the relative reactivity of $Au_3(CO)_2$ and $Au_3(CO)_3$ with O_2. The detailed reactivity of Au_m clusters may still present a theoretical challenge for current quantum chemistry algorithms. Clearly more experimental and theoretical exploration of heavy metal chemistry would be quite important for these advances in our understanding of catalytic chemistry. Based on these results, a complete mechanistic catalytic cycle can be suggested for the gold catalyzed, low temperature oxidation of CO to CO_2. The full cycle is composed of a number of possible elementary reactions.

Acknowledgements

This work is supported by grants from the U.S. DOE BES program, AFOSR, the NSF ERC for Extreme Ultraviolet Science and Technology under NSF Award No. 0310717, and the National Center for Supercomputing Applications under Grant No. CHE090094. The authors would like to thank Profs. Shiv Khanna and Rodney Bartlett, and Dr. Stefan Vajda for helpful discussions concerning gold cluster calculations.

References

[1] M. Haruta, S. Tsubota, T. Kobayashi, H. Kageyama, M.J. Genet, B. Delmon, J. Catal. 144 (1993) 175.
[2] A. Udea, M. Haruta, Gold Bull. 32 (1999) 32.
[3] T. Hayashi, K. Tanaka, M. Haruta, J. Catal. 178 (1998) 566.
[4] S. Arrii, F. Morfin, A.J. Renouprez, J.L. Rousset, J. Am. Chem. Soc. 126 (2004) 1199.
[5] D.C. Meier, D.W. Goodman, J. Am. Chem. Soc. 126 (2004) 1892.
[6] S. Lee, C. Fan, T. Wu, S.L. Anderson, J. Chem. Phys. 123 (2005) 124710.
[7] T.V. Choudhary, D.W. Goodman, Appl. Catal. A 291 (2005) 32.
[8] A.M. Venezia, G. Pantaleo, A. Longo, G.D. Carlo, M.P. Casaletto, F.L. Liotta, G. Deganello, J. Phys. Chem. B 109 (2005) 2821.
[9] M. Arenz, U. Landman, U. Heiz, ChemPhysChem 7 (2006) 1871.
[10] A. Stephen, K. Hashmi, G.J. Hutchings, Angew. Chem. Int. Ed. 45 (2006) 7896.
[11] M.C. Kung, R.J. Davis, H.H. Kung, J. Phys. Chem. C 111 (2007) 11767.
[12] P. Pyykkö, Chem. Soc. Rev. 37 (2008) 1967.
[13] A.A. Herzing, C.J. Kiely, A.F. Carley, P. Landon, G.J. Hutchings, Science 321 (2008) 1331.
[14] J. Gong, C.B. Mullins, Acc. Chem. Res. 42 (2009) 1063.
[15] W.T. Wallace, R.L. Whetten, J. Am. Chem. Soc. 124 (2002) 7499.
[16] J. Hagen, L.D. Socaciu, M. Elijazyfer, U. Heiz, T.M. Bernhardt, L. Wöste, Phys. Chem. Chem. Phys. 4 (2002) 1707.
[17] I. Balteanu, O.P. Balaj, B.S. Fox, M.K. Beyer, Z. Bastl, V.E. Bondybey, Phys. Chem. Chem. Phys. 5 (2003) 1213.
[18] W. Huang, H. Zhai, L.S. Wang, J. Am. Chem. Soc. 132 (2010) 4344.
[19] J.K. Gibson, J. Vac. Sci. Technol. A 16 (1998) 653.
[20] K. Sugawara, F. Sobott, A.B. Vakhtin, J. Chem. Phys. 118 (2003) 7808.
[21] A. Fielicke, G. von Helden, G. Meijer, B. Simard, D.M. Rayner, Phys. Chem. Chem. Phys. 7 (2005) 3906.
[22] M. Neumaier, F. Weigend, O. Hampe, M.M. Kappes, J. Chem. Phys. 122 (2005) 104702.
[23] A. Fielicke, G. von Helden, G. Meijer, D.B. Pedersen, B. Simard, D.M. Rayner, J. Am. Chem. Soc. 127 (2005) 8416.
[24] M. Neumaier, F. Weigend, O. hamper, M.M. Kappes, Faraday Discuss. 138 (2008) 393.
[25] S.M. Lang, T.M. Bernhardt, R.N. Barnett, B. Yoon, U. Landman, J. Am. Chem. Soc. 131 (2009) 8939.
[26] T.H. Lee, K.M. Ervin, J. Phys. Chem. 98 (1994) 10023.
[27] W.T. Wallace, R.L. Whetten, J. Phys. Chem. B 104 (2000) 10964.
[28] H. Häkkinen, U. Landman, J. Am. Chem. Soc. 123 (2001) 9704.
[29] W.T. Wallace, R.B. Wyrwas, A.J. Leavitt, R.L. Whetten, Phys. Chem. Chem. Phys. 7 (2005) 930.
[30] T.M. Bernhardt, L.D. Socaciu-Siebert, J. Hagen, L. Wöste, Appl. Catal. A 291 (2005) 170.
[31] T.M. Bernhardt, J. Hagen, S.M. Lang, D.M. Popolan, L.D. Socaciu-Siebert, L. Wöste, J. Phys. Chem. A 113 (2009) 2724.
[32] A. Fielicke, G. von Helden, G. Meijer, B. Simard, D.M. Rayner, J. Phys. Chem. B 109 (2005) 23935.
[33] L.S. Wang, Phys. Chem. Chem. Phys. 12 (2010) 8694.
[34] W.T. Wallace, R.B. Wyrwas, R.L. Whetten, R. Mitrić, V. Bonačić-Koutecky, J. Am. Chem. Soc. 125 (2003) 8408.
[35] M. Okumura, Y. Kitagawa, M. Haruta, K. Yamaguchi, Chem. Phys. Lett. 346 (2001) 163.
[36] Q. Sun, P. Jena, Y.D. Kim, M. Fischer, G. Ganteför, J. Chem. Phys. 120 (2004) 6510.

[37] M. Okumura, Y. Kitagawa, M. Haruta, K. Yamaguchi, Appl. Catal. A 291 (2005) 37.
[38] D.H. Wells, W.N. Delgass, K.T. Thomson, J. Chem. Phys. 117 (2002) 10597.
[39] X. Wu, L. Senapati, S.K. Nayak, A. Selloni, M. Hajaligol, J. Chem. Phys. 117 (2002) 4010.
[40] A. Prestianni, A. Martorana, F. Labat, I. Ciofini, C. Adamo, J. Phys. Chem. B 110 (2006) 12240.
[41] F. Wang, D. Zhang, X. Xu, Y. Ding, J. Phys. Chem. C 113 (2009) 18032.
[42] A.V. Walker, J. Chem. Phys. 122 (2005) 094310.
[43] M. Ji, X. Gu, X. Li, X. Gong, J. Li, L.S. Wang, Angew. Chem. Int. Ed. 44 (2005) 7119.
[44] S. Gilb, P. Weis, F. Furche, R. Ahlrichs, M.M. Kappes, J. Chem. Phys. 116 (2002) 4094.
[45] J. Li, X. Li, H.J. Zhai, L.S. Wang, Science 299 (2003) 864.
[46] A. Lechtken, D. Schooss, J.R. Stairs, M.N. Blom, F. Furche, N. Morgner, O. Kostko, B. von Issendorff, M.M. Kappes, Angew. Chem. Int. Ed. 46 (2007) 2944.
[47] F. Furche, R. Ahlrichs, P. Weis, C. Jacob, S. Gilb, T. Bierweiler, M.M. Kappes, J. Chem. Phys. 117 (2002) 6982.
[48] F. Tielens, L. Gracia, V. Polo, J. Andrés, J. Phys. Chem. A 111 (2007) 13255.
[49] N. Veldeman, P. Lievens, M. Andersson, J. Phys. Chem. A 109 (2005) 11793.
[50] P. Gruene, D.M. Rayner, B. Redlich, A.F.G. van der Meer, J.T. Lyon, G. Meijer, A. Fielicke, Science 321 (2008) 674.
[51] N. Lopez, J.K. Nørskov, J. Am. Chem. Soc. 124 (2002) 11262.
[52] A. Franceschetti, S.J. Pennycook, S.T. Pantelides, Chem. Phys. Lett. 374 (2003) 471.
[53] N.S. Phala, G. Klatt, E. van Steen, Chem. Phys. Lett. 395 (2004) 33.
[54] X.J. Kuang, X.Q. Wang, G.B. Liu, Catal. Lett. 137 (2010) 247.
[55] Y.P. Xie, X.G. Gong, J. Chem. Phys. 132 (2010) 244302.
[56] B. Assadollahzadeh, P. Schwerdtfeger, J. Chem. Phys. 131 (2009) 064306.
[57] D.H. Wells, W.N. Delgass, K.T. Thomson, J. Catal. 225 (2004) 69.
[58] Y.K. Shi, Z.H. Li, K.N. Fan, J. Phys. Chem. A 114 (2010) 10297.
[59] A.M. Joshi, W.N. Delgass, K.T. Thomson, J. Phys. Chem. B 110 (2006) 2572.
[60] L.D. Socaciu, J. Hagen, T.M. Bernhardt, L. Wöste, U. Heiz, H. Häkkinen, U. Landman, J. Am. Chem. Soc. 125 (2003) 10437.
[61] Q. Xu, L. Jiang, J. Phys. Chem. A 110 (2006) 2655.
[62] T. Davran-Candan, A.E. Aksoylu, R. Yildirim, J. Mol. Catal. A 306 (2009) 118.
[63] D.M. Cox, R. Brickman, K. Creegan, A. Kaldor, Z. Phys. D 19 (1991) 353.
[64] H.J. Zhai, L.S. Wang, J. Chem. Phys. 122 (2005) 051101.
[65] H.J. Zhai, B. Kiran, B. Dai, J. Li, L.S. Wang, J. Am. Chem. Soc. 127 (2005) 12098.
[66] H.J. Zhai, L.L. Pan, B. Dai, B. Kiran, J. Li, L.S. Wang, J. Phys. Chem. C 112 (2008) 11920.
[67] Y.L. Wang, H.J. Zhai, L. Xu, J. Li, L.S. Wang, J. Phys. Chem. A 114 (2010) 1247.
[68] P. Schwerdtfeger, M. Dolg, W.H.E. Schwarz, G.A. Bowmaker, P.D.W. Boyd, J. Chem. Phys. 91 (1989) 1762.
[69] E. Eliav, U. Kaldor, Phys. Rev. A 49 (1994) 1724.
[70] P. Schwerdtfeger, G.A. Bowmaker, J. Chem. Phys. 100 (1994) 4487.
[71] O.D. Häberlen, S.C. Chung, M. Stener, N. Rösch, J. Chem. Phys. 106 (1997) 5189.
[72] N. Bartlett, Gold Bull. 31 (1998) 22.
[73] D.J. Gorin, F.D. Toste, Nature 446 (2007) 395.
[74] W. Huang, M. Ji, C.D. Dong, X. Gu, L.M. Wang, X.G. Gong, L.S. Wang, ACS Nano 2 (2008) 897.
[75] H.S. De, S. Krishnamurty, S. Pal, J. Phys. Chem. C 113 (2009) 7101.
[76] H. Schwarz, Angew. Chem. Int. Ed. 42 (2003) 4442.
[77] M.J. Frisch, G.W. Trucks, H.B. Schlegel, G.E. Scuseria, M.A. Robb, J.R. Cheeseman, J.A. Montgomery, Jr., T. Vreven, K.N. Kudin, J.C. Burant, J.M. Millam, S.S. Iyengar, J. Tomasi, V. Barone, B. Mennucci, M. Cossi, G. Scalmani, N. Rega, G.A. Petersson, H. Nakatsuji, M. Hada, M. Ehara, K. Toyota, R. Fukuda, J. Hasegawa, M. Ishida, T. Nakajima, Y. Honda, O. Kitao, H. Nakai, M. Klene, X. Li, J.E. Knox, H.P. Hratchian, J.B. Cross, V. Bakken, C. Adamo, J. Jaramillo, R. Gomperts, R.E. Stratmann, O. Yazyev, A.J. Austin, R. Cammi, C. Pomelli, J.W. Ochterski, P.Y. Ayala, K. Morokuma, G.A. Voth, P. Salvador, J.J. Dannenberg, V.G. Zakrzewski, S. Dapprich, A.D. Daniels, M.C. Strain, O. Farkas, D.K. Malick, A.D. Rabuck, K. Raghavachari, J.B. Foresman, J.V. Ortiz, Q. Cui, A.G. Baboul, S. Clifford, J. Cioslowski, B.B. Stefanov, G. Liu, A. Liashenko, P. Piskorz, I. Komaromi, R.L. Martin, D.J. Fox, T. Keith, M.A. Al-Laham, C.Y. Peng, A. Nanayakkara, M. Challacombe, P.M. W. Gill, B. Johnson, W. Chen, M.W. Wong, C. Gonzalez, J.A. Pople, Gaussian 03, Revision E.01, Gaussian, Inc., Wallingford, CT, 2004.
[78] ADF2009.01, SCM, Theoretical Chemistry, Vrije Universiteit, Amsterdam, The Netherlands, http://www.scm.com.
[79] H.J. Zhai, C. Bürgel, V. Bonačić-Koutecky, L.S. Wang, J. Am. Chem. Soc. 130 (2008) 9156.
[80] Y. Xie, S.G. He, F. Dong, E.R. Bernstein, J. Chem. Phys. 128 (2008) 044306.
[81] Y. Xie, F. Dong, S. Heinbuch, J.J. Rocca, E.R. Bernstein, Phys. Chem. Chem. Phys. 12 (2010) 947.